School of Mathematical
and Physical Sciences

University of Reading

Department of Mathematics and Statistics

Preprint MPS-2015-18

30 September 2015

Diagnosing observation error correlations for Doppler radar radial winds in the Met Office UKV model using observation-minus-background and observation-minus-analysis statistics

by

J.A. Waller, D. Simonin, **S.L. Dance**, **N.K. Nichols**
and S.P. Ballard

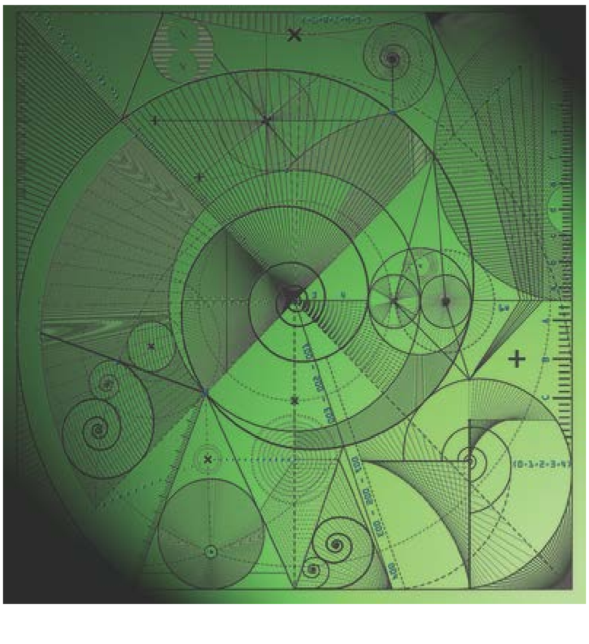

Diagnosing observation error correlations for Doppler radar radial winds in the Met Office UKV model using observation-minus-background and observation-minus-analysis statistics

J. A. Waller[1*], D. Simonin[2], S. L. Dance[1], N. K. Nichols[1], and S. P. Ballard[2]

1. School of Mathematical and Physical Sciences, University of Reading, Reading, Berkshire, RG6 6BB, United Kingdom
2. MetOffice@Reading, Meteorology Building, University of Reading, Reading, Berkshire, RG6 6BB, United Kingdom

September 30, 2015

Abstract

With the development of convection-permitting numerical weather prediction the efficient use of high resolution observations in data assimilation is becoming increasingly important. The operational assimilation of these observations, such as Doppler radar radial winds, is now common, though to avoid violating the assumption of uncorrelated observation errors the observation density is severely reduced. To improve the quantity of observations used and the impact that they have on the forecast will require the introduction of the full, potentially correlated, error statistics. In this work, observation error statistics are calculated for the Doppler radar radial winds that are assimilated into the Met Office high resolution UK model using a diagnostic that makes use of statistical averages of observation-minus-background and observation-minus-analysis residuals. This is the first in-depth study using the diagnostic to estimate both horizontal and along-beam correlated observation errors. By considering the new results obtained it is found that the Doppler radar radial wind error standard deviations are similar to those used operationally and increase as the observation height increases. Surprisingly the estimated observation error correlation length scales are longer than the operational thinning distance. They are dependent on both the height of the observation and on the distance of the observation away from the radar. Further tests show that the long correlations cannot be attributed

*Corresponding Author. Department of Meteorology, University of Reading, Earley Gate, PO Box 243, Reading, RG6 6BB, United Kingdom. email: j.a.waller@reading.ac.uk

to the use of superobservations or the background error covariance matrix used in the assimilation. The large horizontal correlation length scales are, however, in part, a result of using a simplified observation operator.

1 Introduction

With the recent development of convection permitting numerical weather prediction (NWP), such as the Met Office UK variable resolution (UKV) model [Lean et al., 2008, Tang et al., 2013], the assimilation of observations that have high frequency both in space and time has become increasingly important [Park and Zupanski, 2003, Dance, 2004, Sun et al., 2014, Ballard et al., 2015, Li et al., 2015]. The potential for assimilating one such set of observations, the Doppler radar radial winds (DRWs) [Lindskog et al., 2004, Sun, 2005], has been explored by a number of operational centers e.g., Lindskog et al. [2001], Salonen et al. [2007], Rihan et al. [2008], Salonen et al. [2009]. The assimilation of the DRWs has been shown to provide a significant positive impact on the forecast [Xiao et al., 2005, Lindskog et al., 2004, Montmerle and Faccani, 2009, Simonin et al., 2014] and as a result they are now included in operational assimilation [Xiao et al., 2008, Simonin et al., 2014].

Currently at the Met Office the error statistics associated with DRWs are assumed uncorrelated [Simonin et al., 2014]. To reduce the large quantity of data and ensure the assumption of uncorrelated errors is reasonable the DRW observations are 'superobbed' and thinned before assimilation [Simonin et al., 2014]. These processes result in a large number of observations being discarded. Having accurate estimates of the error statistics that are well understood and correctly represented in the assimilation will allow better use of the observational data.

The errors associated with the observations can be attributed to four main sources:

1. Instrument error.
2. Error introduced in the observation operator - including omissions in the observation operator e.g. the misrepresentation of the radar beam bending, and errors due to the approximation of a continuous function as a discrete function.
3. Errors of representativity - errors that arise where the observations can resolve spatial scales that the model cannot.
4. Pre-processing errors - errors introduced by pre-processing such as clutter removal.

For DRWs the instrument errors are independent and uncorrelated. Observation error correlations, which may be state dependent and dependent on the model resolution, are likely to arise from the other sources of error [Janjic and Cohn, 2006, Waller, 2013, Waller et al., 2014a,b]. The inclusion of correlated observation errors in the assimilation has been shown to lead to a more accurate analysis, the inclusion of more observation information content and improvements in the forecast skill score [Stewart et al., 2013, Stewart, 2010, Healy and White, 2005, Stewart et al., 2008, Weston et al., 2014]. Significant benefit may even be provided by using only a crude approximation to the observation error covariance matrix [Stewart et al., 2013, Healy and White, 2005].

A number of methods exist for estimating the observation error covariances e.g. Hollingsworth and Lönnberg [1986], Dee and Da Silva [1999]. Xu et al. [2007] presented an innovation method based on that of Hollingsworth and Lönnberg [1986] for estimating DRW error and background wind error covariances. Simonin et al. [2012] previously calculated observation error statistics for DRWs using the method of Xu et al. [2007]. The work of Simonin et al. [2012] suggests that the observation error standard deviation increases with the height of the observation and that the observations errors have a correlation length scale of 1-3km. However, the Hollingsworth and Lönnberg [1986] method was designed to provide estimates of the background error statistics under the assumption of uncorrelated observation errors. When using the method to estimate both correlated background and correlated observation errors, determining how to split the estimated quantity into observation and background errors is non-trivial [Bormann and Bauer, 2010]. Indeed the result is subjective. To overcome this difficulty most recent attempts to diagnose the observation error correlations have made use of the diagnostic proposed in Desroziers et al. [2005]. Initially designed as a consistency check, the diagnostic provides an estimate of the observation error covariance matrix using the statistical average of observation-minus-background and observation-minus-analysis residuals. However, in theory it relies on the use of exact background and observation error statistics in the assimilation. Despite this limitation, the diagnostic has been used to estimate inter-channel observation error statistics [Stewart et al., 2009, 2014, Bormann and Bauer, 2010, Bormann et al., 2010, Weston et al., 2014] even when the error statistics used in the assimilation are not exact. The method of Desroziers et al. [2005] has also been used by Wattrelot et al. [2012] to calculate observation error statistics for the Doppler radial winds assimilated into the Météo-France system. Their results, published as a conference paper, show a similar error standard deviation to those found in Simonin et al. [2012], but suggest that the observation errors have a larger correlation length scale of approximately 10km. (we cannot determine the length scale precisely due the data thinning they have applied).

Here we present the first in-depth study using the diagnostic of Desroziers et al. [2005] to calculate observation error statistics for the DRWs assimilated into the Met Office high resolution UK (UKV) model. We consider the sensitivity of the estimated observation error statistics to the choice of assimilated background error statistics, the use of superobservations and the use of a more sophisticated observation operator. We find that the DRW error standard deviations are similar to those used operationally, though surprisingly, the observation error correlation length scales are longer than the operational thinning distance. Further tests show that the long correlations cannot be attributed to the use of superobservations or the background error covariance matrix used in the assimilation. The large horizontal correlation length scales are, however, in part, a result of using a simplified observation operator in the assimilation.

This paper is organised as follows. In Section 2 we give a description of the diagnostic of

Desroziers et al. [2005]. We describe the DRW observations and their model representations in Section 3 and in Section 4 we describe the experimental design. In Section 5 we consider the estimated observation error statistics from four different cases. Finally we conclude in Section 6.

2 The diagnostic of Desroziers et al. [2005]

Data assimilation techniques combine observations $\mathbf{y} \in \mathbb{R}^{N^p}$ with a model prediction of the state, the background $\mathbf{x}^b \in \mathbb{R}^{N^m}$, often determined by a previous forecast. Here N^p and N^m denote the dimensions of the observation and model state vectors respectively. In the assimilation the observations and background are weighted by their respective errors, using the background and observation error covariance matrices $\mathbf{B} \in \mathbb{R}^{N^m \times N^m}$ and $\mathbf{R} \in \mathbb{R}^{N^p \times N^p}$, to provide a best estimate of the state, $\mathbf{x}^a \in \mathbb{R}^{N^m}$, known as the analysis. To calculate the analysis the background must be projected into the observation space using the possibly non-linear observation operator, $\mathcal{H} : \mathbb{R}^{N^p} \rightarrow \mathbb{R}^{N^m}$. After an assimilation step the analysis is evolved forward in time to provide a background for the next assimilation.

Desroziers et al. [2005] assume that the analysis is determined using,

$$\mathbf{x}^a = \mathbf{x}^b + \mathbf{K}(\mathbf{y} - \mathcal{H}(\mathbf{x}^b)), \tag{1}$$

where $\mathbf{H}$ is the observation operator linearised about the current state and $\mathbf{K} = \mathbf{B}\mathbf{H}^T(\mathbf{H}\mathbf{B}\mathbf{H}^T + \mathbf{R})^{-1}$ is the gain matrix.

The diagnostic described in Desroziers et al. [2005] estimates the observation error covariance matrix by using the observation-minus-background and observation-minus-analysis residuals. The background residual,

$$\mathbf{d}_b^o = \mathbf{y} - \mathcal{H}(\mathbf{x}^b), \tag{2}$$

is the difference between the observation $\mathbf{y}$ and the mapping of the forecast vector, $\mathbf{x}^b$, into observation space by the observation operator $\mathcal{H}$. The analysis residual,

$$\begin{aligned} \mathbf{d}_a^o &= \mathbf{y} - \mathcal{H}(\mathbf{x}^a), & (3) \\ &\approx \mathbf{y} - \mathcal{H}(\mathbf{x}^b) - \mathbf{H}\mathbf{K}\mathbf{d}_b^o. & (4) \end{aligned}$$

is similar to the background residuals, but with the forecast vector replaced by the analysis vector $\mathbf{x}^a$. By taking the statistical expectation of the product of the analysis and background residuals results in

$$E[\mathbf{d}_a^o \mathbf{d}_b^{oT}] \approx \mathbf{R}, \tag{5}$$

assuming that the forecast and observation errors are uncorrelated. Equation (5) is exact if the observation and background error statistics used in assimilation are exact. The theoretical work of Waller et al. [2015] provides insight on how results from the diagnostic can be interpreted when the incorrect background and observation error statistics are used in the assimilation. Due to the statistical nature of the diagnostic the resulting matrix will not be symmetric. Therefore, if the matrix is to be used it must be symmetrised.

3 Doppler Radar radial wind observations and their model representation

3.1 The Met Office UKV model and 3D variational assimilation scheme

The operational UKV model is a variable resolution convection permitting model that covers the UK [Lean et al., 2008, Tang et al., 2013]. The model has 70 vertical levels. The horizontal grid has a 1.5km fixed resolution on the interior surrounded by a variable resolution grid which increases smoothly in size to 4km. The variable resolution grid allows the downscaled boundary conditions, taken from the global model, to spin up before reaching the fixed interior grid. The initial conditions are provided from a 3D variational assimilation scheme that uses an incremental approach [Courtier et al., 1994] and is a limited-area version of the Met Office variational data assimilation scheme [Lorenc et al., 2000, Rawlins et al., 2007]. The assimilation uses an adaptive mesh, that allows the accurate representation of boundary layer structures [Piccolo and Cullen, 2011, 2012] . The background error covariance statistics used in this study are described in Section 4.

3.2 Doppler radar radial wind data

Doppler radar is an active remote sensing instrument that provides observations of radial wind by measuring the phase shift between a transmitted electromagnetic wave pulse and its backscatter echo. The radial velocity of a scattering target is then estimated from the 'Doppler shift' [Doviak and Zrnic, 1993]. While it is possible to derive clear air radar returns e.g. Rennie et al. [2010, 2011], in this work we consider only observations where the scattering targets are assumed to be raindrops. The DRW data used at the Met Office are acquired using 18 C-Band weather radars. Each radar completes a series of scans out to a range of 100km every 5 minutes at different elevation angles (typically 1^o, 2^o, 4^o, 6^o and 9^o) with a $1^o \times 600$m resolution volume. Before being assimilated the data is processed and a quality control procedure is applied. This ensures that no observations that disagree with neighboring observations or have a large departure from the background are assimilated. The observations errors are assumed Gaussian and uncorrelated in space or time with standard deviations that range from $1.8ms^{-1}$ for observations close to the radar to $2.8ms^{-1}$ for observations furthest away from the radar. Further details of the operational assimilation of DRWs at the Met Office can be found in Simonin et al. [2014].

3.2.1 The current operational observation operator

To compare the background with the observations it is necessary to map the model state into observation space. The current operational observation operator, following Lindskog et al. [2000], first interpolates the NWP model horizontal and vertical wind components u, v and w to the observation location. The horizontal wind is then projected in the direction of the radar beam and projected onto the slant of the radar beam using,

$$v_r = (u \sin\phi + v \cos\phi)\cos(\theta) + w \sin(\theta), \tag{6}$$

where ϕ is the radar azimuth angle clockwise from due north and θ is the beam center elevation angle. The elevation angle $\theta = \epsilon + \alpha$ includes a correction term, α, that must be added to the measurement elevation angle ϵ. The correction term

$$\alpha = \tan^{-1}\left(\frac{r\cos(\epsilon)}{r\sin(\epsilon) + a_e + h_r}\right), \tag{7}$$

where h_r is the height of the radar above sea level, r is the range of the observation and a_e is the effective earth radius (1.3 times the actual earth radius) required to take account of the earth's curvature and the radar beam refraction [Doviak and Zrnic, 1993]. The correction term is not exact. The value of a_e is only valid in the international standard atmosphere. This simple operational observation operator does not account for the beam broadening or reflectivity weighting. Additionally, only the horizontal wind components are updated in the minimisation, the vertical component of wind remains at its fixed background value.

This operational observation operator is used in the majority of results discussed in this article.

3.2.2 An improved observation operator

In recent research experiments the Met Office trialed a more sophisticated observation operator [Simonin, 2014]; it includes a beam broadening model, as well as a weighting with reflectivity. The beam broadening model, W_{bb}, takes the form,

$$W_{bb}(\theta_z) = exp(-2ln\left(\frac{\theta_z^2}{\theta_{3dB}^2}\right)), \tag{8}$$

with $\theta_z^2 = \theta^2 - \theta_b^2$ where θ is the beam centre elevation as in equation (6), θ_b is the lower beam elevation (the lower limit of the beam spread) and θ_{3dB} is the half power bandwidth (angular range of the antenna pattern in which at least half of the maximum power is still emitted [Toomay and Hannen, 2004]). For the reflectivity weighting, a climatological profile with height h is used,

$$W_{ref}(h) = Zh + c, \tag{9}$$

where,

$$Z = \begin{cases} -6dB : h < Brightband_L \\ -2dB : h > Brightband_U \end{cases}, \tag{10}$$

c is a constant scaling factor, $Brightband_L$ is the lower limit of the Bright band and $Brightband_U$ is the upper limit of the Bright band. The height of the Bright band (a layer of melting ice resulting in intense reflectivity return [Kitchen, 1997]) is derived from the forecast model temperature field, and has a thickness set to 250m. The reflectivity profile increases by 10dB from the bottom to the centre of the bright band and then decreases linearly. The beam broadening and reflectivity weighting are combined to give a single weight, $W = W_{ref}W_{bb}$ and this weighting is included in the new observation operator,

$$v_r = \sum_{\theta_{beam}} W(u \sin\phi + v \cos\phi)\cos(\theta). \tag{11}$$

The implementation of this new observation operator has been shown to reduce the error in the background residuals. This new observation operator may be further improved [Fabry, 2010], though the operational use of a more complex observation operator may not be feasible. While these simplifications and omissions in the observation operator exist, they will introduce additional error when the model background is projected into observation space. These errors may well be correlated and should ideally be accounted for in the observation error covariance matrix.

3.2.3 Superobservation creation

To reduce the density of the observations, multiple observations are made into a single superobservation. Only observations that have passed the quality control procedure described in Simonin et al. [2014] are combined to make the superobservations. There are a number of methods for calculating the superobservations. The Doppler radar superobservations used at the Met Office are calculated following the method of Salonen et al. [2008]. The radar scan is divided into 3^o by $3km$ cells and one observation is created per cell using the following procedure:

1. Project background winds into observation space using equation (6);
2. Calculate the background residual at each observation location;
3. Average all background residuals that fall within a superobservation cell;
4. Add the average residual to the simulated background radial wind at the center of the superobservation cell to give a value for the superobservation.

The calculated superobservations are subject to a second quality control procedure [Simonin et al., 2014]. They are then further thinned to 6km, where is assumed that the observations will have uncorrelated error, using Poisson disk sampling [Bondarenko et al., 2007].

3.2.4 Superobservation error

The calculated superobservations have an associated superobservation error, ϵ^{so}. Berger and Forsythe [2004] showed that the covariance of the superobservation error will be equivalent to the averaged observation error covariance matrix for the raw observations (i.e.

creating the superobservations using the background does not introduce any background error into ϵ^{so}) if:

1. The observation and background errors are independent;
2. The background state errors are fully correlated within the superobservation cell;
3. The background state errors in a superobservation cell all have the same magnitude and
4. The background residuals are equally weighted within a superobservation cell.

However, for DRWs it is not clear that all the assumptions will hold. In particular assumptions 1 and 2 are valid at close range to the radar where the superobservation cells are small. However, at far range the superobservation cells are large and the assumptions are likely to be invalid. Therefore, it is possible that at large ranges there is a small influence of the background errors on the error associated with the superobservation.

4 Experimental Design

To calculate estimates of the observation error covariances we require background and analysis residuals. Results from four different assimilation runs are considered, all use background, $\mathbf{d}^o_b$, and analysis, $\mathbf{d}^o_a$, residuals from June, July and August 2013. Observations in this study come from 9 of the 18 radars in the network.

Case 1 uses residuals produced by running the UKV under the January 2014 operational set up. This uses superobservations (calculated as described in Section 3.2.3) thinned to 6km and the observation operator given in equation (6). The background error covariance ('New') has been derived using the Covariances and VAR Transforms (CVT) software which is the new Met Office covariance calibration and diagnostic tool that analyses training data representing forecast errors (either using the so-called NMC lagged forecast technique or ensemble perturbations). Here a NMC method has been applied to (T+6 hour)-(T+3 hour) forecast differences to diagnose a variance and correlation length scale for each vertical mode.

Case 2 considers the effect of using the old operational (used prior to January 2013) UKV background error covariance matrix ('Old'). These statistics were generated from (T+24 hour)-(T+12 hour) forecast differences and, contrary to the CVT approach, the correlation functions used specific fixed length scales [Ballard et al., 2015]. This background error covariance matrix has larger variances than the matrix used in Case 1 and the correlations length scales are slightly longer.

Case 3 uses the same background error covariance as Case 1, but used raw observations (thinned to 6km) rather than using the superobservations.

Case 4 uses the same design as Case 3, but the operational observation operator is replaced with the observation operator described in equation (11). We summarise the different cases in Table 1.

Table 1 – Summary of experimental design for different cases

Case	**B**	Superobservations	Observation Operator
1	New	Yes	Old
2	Old	Yes	Old
3	New	No	Old
4	New	No	New

For each case the available data for each radar scan is stored in 3D arrays of size $N^s \times N^r \times N^a$ where N^s is the number of scans containing data, $N^r = 16$ is the number of ranges and $N^a = 120$ is the number of azimuths. Figure 1 shows a radar scan with the typical superobservation cells. The data is also separated by elevation, with data available at elevation angles 1^o, 2^o, 4^o and 6^o. (We do not estimate the observation error statistics for the 9^o beam due the lack of avaliable data). The position of these observations at these elevations are shown in Figure 2, we note that the color scheme for each given elevation is used throughout the figures in this manuscript. It is important to note that these observations are only available in areas where there is precipitation and it is possible that only part of the scan contains observations. Furthermore, the use of the superobservations, thinning and quality control results in a limited amount of data in each scan. The amount of data available differs for each elevation, with data for the lower elevations available at far range, and for higher elevations available for near range. This lack of data means that standard deviations and correlations are not available for every range at each elevation. Results are not plotted for standard deviations unless 1500 samples were available; for correlations the required number of samples is 500. Observations may be correlated along the beam, horizontally or vertically. Here we consider both horizontal correlations and those along the beam.

Horizontal correlations consider how observations at a given height are correlated. The blue cells in Figure 1 show a set of observations that would be compared for a given height. For each radar scan, data is sorted into 200m height bins. Here the height takes into account the height of the radar above sea level. All observations that fall into a particular height bin are considered. The data is binned by separation distance for each pair of observations and from this the correlations are calculated.

When calculating along-beam correlations we consider how observations in the same beam are correlated to each other, where correlations are expressed for the separation distance along the beam. The red cells in Figure 1 show one set of observations that would be considered in this case. Here the samples used for calculating equation (5) are taken to be the individual scans along the azimuth. Samples are taken on all dates, from all radars and from each azimuth. When calculating results along the beam we do not expect to obtain symmetric correlation functions. When considering the along-beam correlations at any given range the positive separation distance will result in a different correlation to the negative separation distance. For example, say we are considering the correlations for

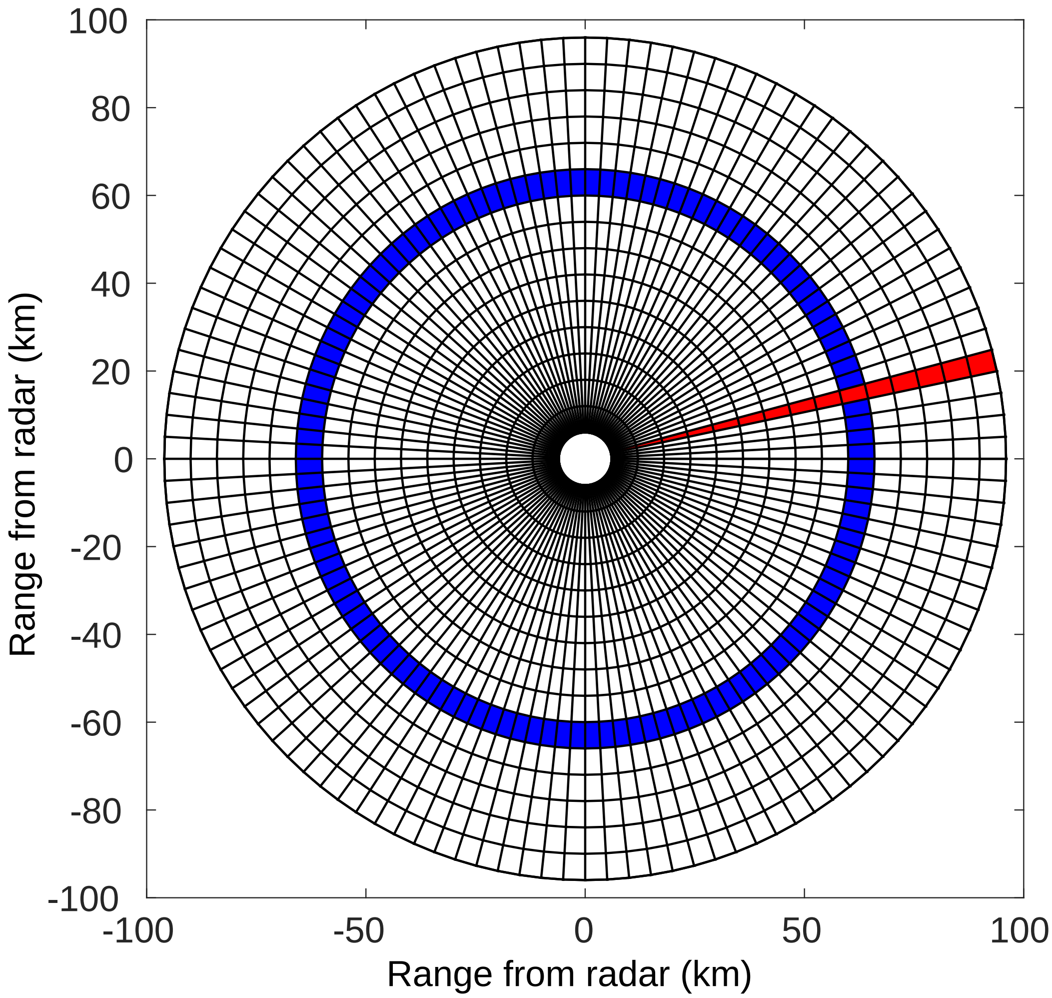

Figure 1 – A typical radar scan where each box is the location of a superobservation. The blue cells show a group of observations, all at the same height, that would be compared to calculate horizontal correlations. The red cells show observations that would be compared to calculate the along-beam correlations.

the observation located at 30km range, the correlation with the 18km observation (-12km separation) will have a smaller measurement volume whereas the observation at 42km (+12km separation) will have a larger measurement volume. This is an important factor to consider when analysing the along-beam correlation results.

For both horizontal and along-beam correlations it is possible to calculate an average correlation function using all available data that is homogeneous for all elevations, heights and ranges. These average correlation functions provide an overall impression of how the calculated covariance differs between cases. The average along-beam correlation functions are also comparable to those calculated in Wattrelot et al. [2012]. The disadvantage of this method is that different elevations represent different heights in the atmosphere, and also have interaction with different model levels. Therefore it is difficult to distinguish how the error correlations arise, whether they are a result of errors in the observation operator, or arise from the misrepresentation of scales. In an attempt to understand exactly what is contributing to the error we also calculate the correlations for different elevations separately as this allows us to better understand the origin and behaviour of the errors.

5 Results

5.1 Case 1 - Results from the operational system

We begin by calculating the observation error covariances for Case 1. Here data was acquired using the January 2014 operational system. This uses superobservations (calculated as described in Section 3.2.3) thinned to 6km, the observation operator given in equation (6) and the 'new' background error covariance statistics.

5.1.1 Horizontal correlations

We first calculate the average horizontal correlation function using all data from all elevations. We show the standard deviation for this case in Table 2 and the correlation in Figure 3. (Note that the table and figure contain results for all cases; in this section we discuss the results for Case 1 only). The standard deviation falls within the range of operational DRW standard deviations. We see that the correlation length scale (defined to be the distance at which correlation becomes insignificant (< 0.2) [Liu and Rabier, 2002]) is approximately 24km. This is much larger than the distance calculated in Simonin et al. [2012] (1-3km) and the operational thinning distance of 6km. This indicates that the assumption of uncorrelated errors is incorrect.

We now consider the horizontal correlations for different heights and each elevation separately. In Figure 4 we plot the standard deviation with height for each elevation. We see that the standard deviations increase with height with the exception of the lowest levels, and are similar for each elevation. For each elevation the volume of atmosphere sampled by

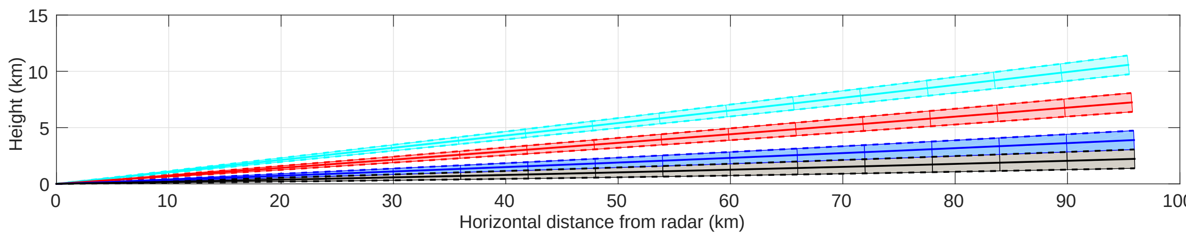

Figure 2 – A typical radar beam at elevations 1^o (black), 2^o (blue), 4^o (red) and 6^o (cyan).

Table 2 – Horizontal and along-beam standard deviations calculated for Cases 1-4 using all available data up to a height of 5km.

Case	Horizontal standard deviation (ms^{-1})	Along-Beam standard deviation (ms^{-1})
1	1.97	1.95
2	1.57	1.59
3	1.96	1.99
4	1.82	1.89

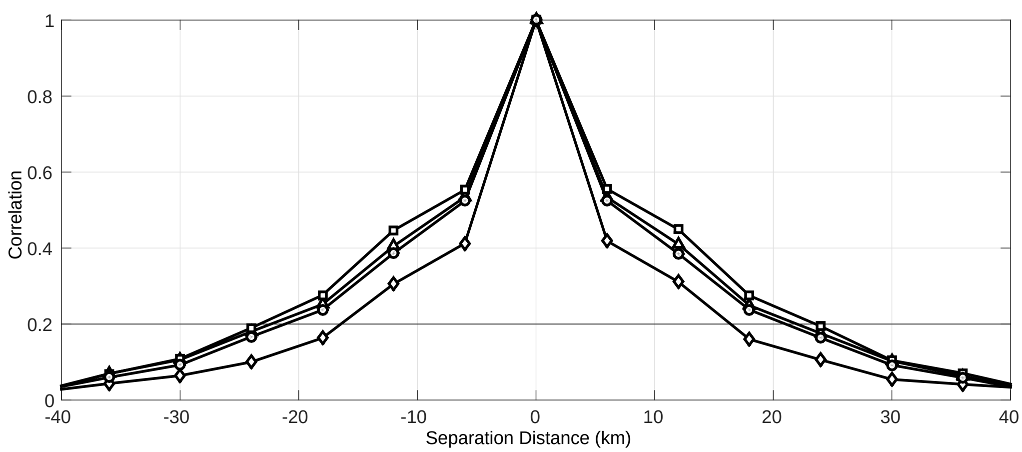

Figure 3 – All elevation horizontal observation error correlations for Case 1 (Control, squares), Case 2 (Alternate background error statistics, diamonds), Case 3 (Thinned raw data, triangles) and Case 4 (New observation operator, circles) . Error correlations are deemed to be insignificant below the horizontal line at 0.2.

the observation increases with height. (Note that at any given height the volume sampled by the 6^o beam will be smaller than the 1^o beam). Observations that sample larger volumes are expected to have a larger instrument error as the Doppler shift is calculated from multiple scattering targets in the measurement volume. In addition these observations will be subject to more error from the observation operator as only information from the model level nearest to the centre of the sample volume is utilised, even when the sample volume spans several model layers. The increased errors at the lowest height may be a result of larger representativity errors as the observations at the lower heights sample smaller volumes than the model resolution. Our results support previous work in Simonin et al. [2014] and we find that the standard deviations are similar to those used operationally.

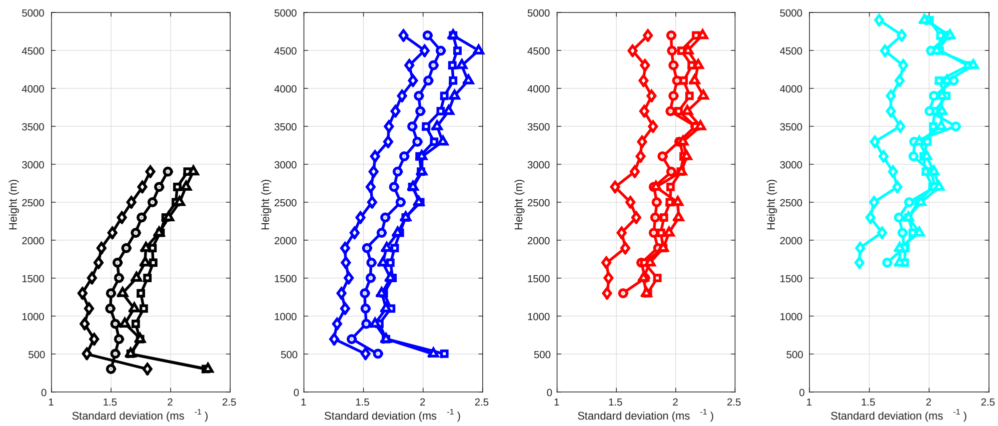

Figure 4 – Horizontal observation error standard deviation for elevations 1^o (black), 2^o (blue), 4^o (red) and, 6^o (cyan) for Case 1 (Control, squares), Case 2 (Alternate background error statistics, diamonds), Case 3 (Thinned raw data, triangles) and Case 4 (New observation operator, circles).

Next we consider how the horizontal correlation length scale changes for a given elevation at different heights. We plot the calculated correlation functions for a range of heights in Figure 5. We see that the correlation length scale increases with height and ranges between 17km and 32km. For all heights the correlation length scale is longer than the operational thinning distance. An increase in height corresponds to an increase in both the distance of observation away from the radar and the volume of the measurement box and therefore the change in correlation length scale could be attributed to either of these variables.

In an attempt to determine the cause of the change in length scale we consider the horizontal correlations at the 2.5km height for the different elevations. At any given height the measurement volume of the observation is larger for lower elevations. Figure 6 shows that the correlation length scales are larger for the lower elevations. This suggests that it is the change in measurement volume that affects the correlation length scale. As in this case the observation operator does not account for the observation volume, it is likely that the correlated error is, in part, caused by the error in the observation operator.

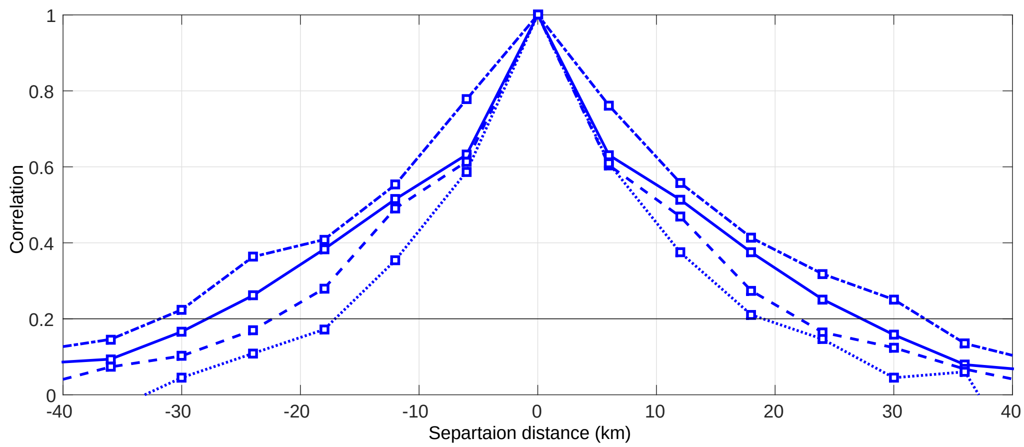

Figure 5 – Horizontal observation correlations for elevation 2^o at height 1.1km (dot), 2.7km (dash), 3.5km (solid) and 4.3km (dot-dash) for Case 1 (control). Error correlations are deemed to be insignificant below the horizontal line at 0.2.

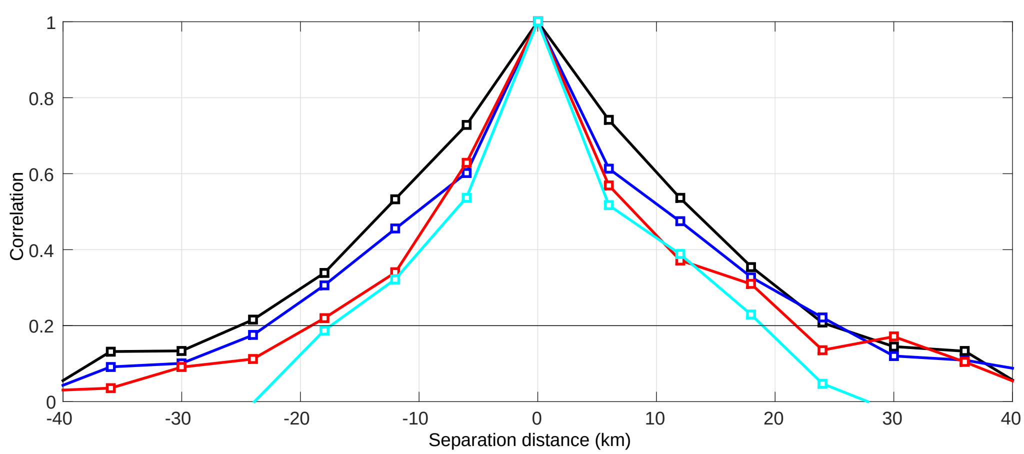

Figure 6 – Horizontal correlations at height 2.5km for elevations 1^o (black), 2^o (blue), 4^o (red) and, 6^o (cyan) for Case 1 (Control). Error correlations are deemed to be insignificant below the horizontal line at 0.2.

It is also possible to compare observations at the same range, observations will have the same measurement volume but will be at different heights in the atmosphere. In this case we find that for each elevation the correlation length scale is similar, e.g. at a range of 40km each elevation has a correlation length scale of $\approx$ 23km (not shown). This suggests that the the measurement volume of the observation has the largest impact on the horizontal correlation length scale, with correlation length scale increasing with measurement volume.

5.1.2 Along-beam correlations

Next we calculate the along-beam observation errors using the data from Case 1. We begin by calculating the average observation error covariance and comparing these results with those from Météo-France [Wattrelot et al., 2012]. We do not expect estimated statistics to be equal to those found by Météo-France as there are differences in the operational set up (e.g. observation and background error covariance statistics, observation processing, observation operators and thinning distances) and the region and time scale covered by the data.

Our estimated standard deviation (Table 2) is larger than the standard deviation found by Météo-France which is $1.51ms^{-1}$. This is likely to be the result of the different operational set up and observation processing. We plot our estimated correlation function along with the correlation found by Météo-France in Figure 7. We see that the correlation

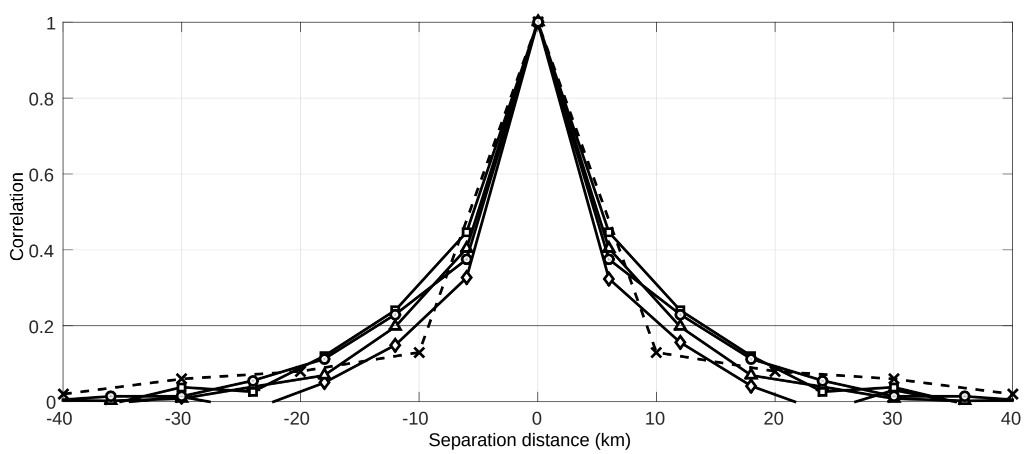

Figure 7 – All elevation along-beam observation error correlation for Cases 1 (Control, squares), 2 (Alternate background error statistics, diamonds), 3 (Thinned raw data, triangles) and 4 (New observation operator, circles) and those found previously by Météo-France (crosses). Error correlations are deemed to be insignificant below the horizontal line at 0.2.

length scales are approximately $5km$ longer than those found by Météo-France. Given the different operational setup used by Météo-France the similarities between the results are reassuring and suggest that we are obtaining a reasonable estimate of the observation error correlations.

Next we calculate the error statistics along the beam for each elevation. In Figure 8 (square symbols) we plot the change in standard deviation with height for beam elevations 1^o, 2^o, 4^o and 6^o. (For the horizontal correlations the height of the radar above sea level was accounted for; here height is calculated assuming that the radar is at sea level). For all

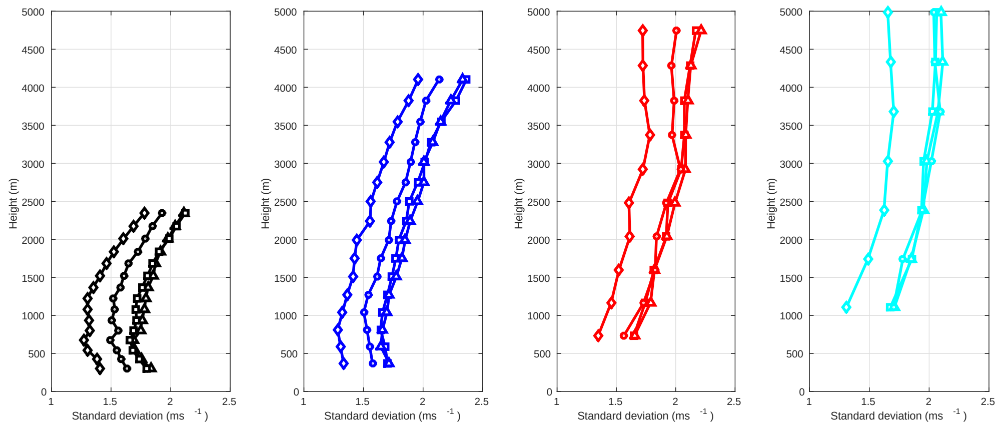

Figure 8 – Along-beam observation error standard deviation for elevations 1^o (black), 2^o (blue), 4^o (red) and, 6^o (cyan) for Case 1 (Control, squares), Case 2 (Alternate background error statistics, diamonds), Case 3 (Thinned raw data, triangles) and Case 4 (New observation operator, circles).

elevations the observation error standard deviation generally increases with height, with the exception of the lowest levels. This is similar to the behaviour of the standard deviations for the horizontal case. Unlike the horizontal case the standard deviations for each elevation are not so similar. For any given height the standard deviations are larger for the lower elevations. At any given height the lower elevations will be sampling larger volumes of the atmosphere. Observations sampling large volumes are subject to both larger instrument error and more error in the observation operator.

We now consider how the correlation length scale changes for a given elevation at different heights. The estimated observation error correlations for a range of heights are plotted in Figure 9. The along-beam correlation length scales are shorter than the horizontal correlations, though the correlation length scale still increases with height for any given elevation. This highlights the relationship between the increase in correlation length scale with the increasing height, range and volume measurement of the observation.

In Figure 10 we consider how the correlation function differs with measurement volume. We plot the along-beam correlation function for each elevations at a height of 2.5km. Here the height for each observation is the same, but the measurements are taken at different ranges with the lowest elevation at the furthest range. Figure 10 shows that the correlation

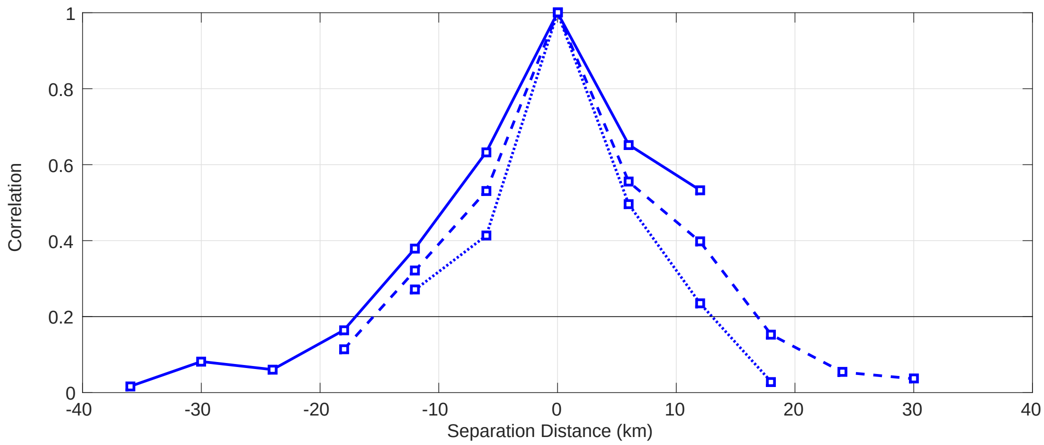

Figure 9 – Along-Beam observation correlations for elevation 2^o at height 1.1km (dotted line), 3.0km (dashed line) and 3.5km (solid line) for Case 1 (Control).

length scale increases with range. Again this likely to be a result of the larger measurement volumes at far range.

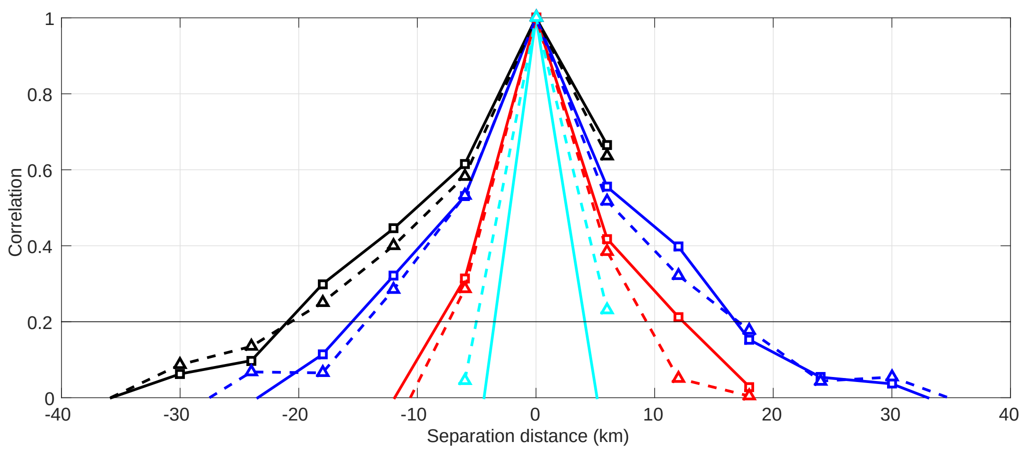

Figure 10 – Correlations along the beam at height 2.5km for elevations and approximate ranges $1^o \approx 100$km (black), $2^o \approx 64$km (blue), $4^o \approx 35$km (red) and , $6^o \approx 22$km (cyan) for superobbed data (squares/solid lines) and thinned raw data (triangles/dashed lines). Error correlations are deemed to be insignificant below the horizontal line at 0.2.

In Figure 11 we plot the correlation function for each elevation at a range of 40km. Here the volume of measurement for each observation is the same, but measurements from lower elevations are at lower heights. We see that the correlation length scale differs with elevation and decreases with height. We hypothesise that the change in correlation is a result of the different levels of the atmosphere sampled by different beam elevations. For the low elevation angles the beam gradient is shallow, hence different gates measure similar heights in the atmosphere; this results in larger error correlations. Larger elevation angles have larger beam gradients, different gates sample a wider range of heights in the atmosphere; this results in small observation error correlations.

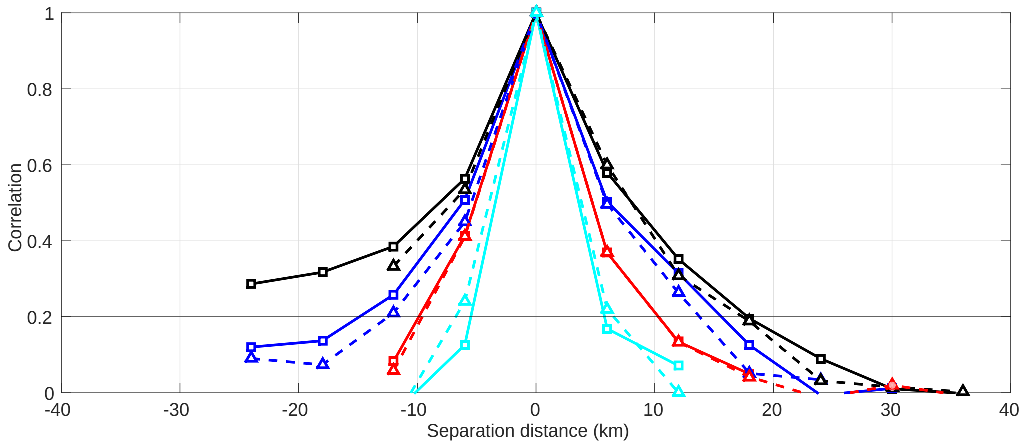

Figure 11 – Correlations along the beam at range 40km for elevations and approximate heights $1^o \approx 0.8$km (black), $2^o \approx 1.5$km (blue), $4^o \approx 3.0$km (red) and , $6^o \approx 4.3$km (cyan) for superobbed data (solid lines) and thinned raw data (dashed lines). Error correlations are deemed to be insignificant below the horizontal line at 0.2.

5.1.3 Summary

For this case we have calculated observation error statistics using data from the January 2014 operational UKV model and assimilation. We find that:

- DRW standard deviations increase with height (with the exception of the lowest heights). This is likely due to the increasing measurement volume with height. The larger errors at the lowest height are likely to be a result of representativity errors.
- The correlation length scale is larger than the thinning distance of 6km chosen to ensure that the assumption of uncorrelated errors is valid.
- For both horizontal and along-beam correlations and for all elevations the observation error correlation length scale increases with height. We hypothesise that this is in part due to the larger errors in the observation operator and correlated superobservation errors at large range. This will be the subject of further investigation (see sections 5.3 and 5.4).

5.2 Case 2 - The effect of changing the assimilated background error statistics

The diagnostic of Desroziers et al. [2005] uses the assumption that the observation and background error covariance matrices used in the assimilation are exact. In the operational assimilation, Case 1, the observation errors are assumed uncorrelated and the background error variance and correlation length scale are believed to be too large. Results given in Waller et al. [2015] relating to the diagnostic suggest that under these circumstances the diagnostic will underestimate the observation error correlation length scale. Therefore it is possible that the true observation error statistics have longer correlation lengths than those calculated for Case 1.

To provide information on how results in Case 1 may compare to the true observation error statistics, we consider the sensitivity of the estimated observation error statistics to using different background statistics. Here we use previous operational background error statistics that have larger variances and larger length scales than the background error statistics used in the previous experiments.

5.2.1 Horizontal correlations

The average standard deviation given in Table 2 shows that the use of background error statistics with larger variance and longer length scales results in a lower estimate of the observation error standard deviation. The correlation function, plotted in Figure 3, shows clearly that using a different background error covariance matrix has reduced the estimated observation error correlation length scale. These results agree with the theoretical results in Waller et al. [2015] (larger overestimates of variance and correlation length scale in the assimilated background statistics results in more severe underestimates of observation error variance and correlation length scale) and suggest that the theoretical results developed under simplifying assumptions are still applicable in an operational setting. The theoretical work and results from Cases 1 and 2 suggest that if the variances and length scales in the assumed covariance matrix $\mathbf{B}$ were further reduced compared to Case 1, the estimated observation error correlation length scales would be larger.

Figure 4 shows that the change in standard deviation with height for each elevation is similar to Case 1. However, the standard deviations for Case 2 are smaller than those from Case 1, a result of the larger background error variances used in the assimilation.

As with the average correlations, results relating to the correlations for each individual elevation and height have smaller correlation length scales than Case 1 (not shown). However, we still find that the qualitative behaviour of the correlation length scales remains the same; that is, for any elevation the correlation length scale increases with height and for any given height the length scale decreases as elevation increases.

5.2.2 Along-beam correlations

For the average along-beam correlation we find the standard deviation (Table 2) is reduced compared to Case 1. The correlations plotted in Figure 7 also have a shorter length scale (approximately 10km) and are more comparable to those found by Météo-France.

When considering the standard deviations for each elevation we again see that they are reduced (see diamonds Figure 8). Though the change in standard deviation with height is qualitatively similar to Case1. We find that the the shape of the correlation function is similar, but the length scales are shorter than those calculated in Case 1 (not shown). The variation in the correlation length scale with elevation, height and range is, however, unaltered.

5.2.3 Summary

For this case we have calculated observation error statistics using different background error statistics which have larger variances and correlation length scales. We find that:

- Estimated observation error standard deviations (length scales) are smaller (shorter) when using the alternative background error statistics. However, changes in standard deviation and correlation length scale with height remain qualitatively similar to Case 1.
- Results from Case 1 and Case 2 follow the theoretical work of Waller et al. [2015]. Given that the standard deviation and background statistics in Case 1 are believed to be too large (though smaller than Case 2), it is possible that the true error statistics have larger standard deviations and longer length scales than those calculated in Case 1.

5.3 Case 3 - The effect of the superobservations

The creation of the superobservations, discussed in section 3.2.3, results in an observation error that is only independent of the background error if the errors in the background states used in the calculation of each superobservation are of the same magnitude and are fully correlated [Berger and Forsythe, 2004]. This assumption is true at close range to the radar, but it is possible that it is violated at far range resulting in increased observation error correlation length scales. To determine if the superobservations have this effect we consider the results from Case 3, where the assimilation uses thinned raw data. We return to using the 'New' background error statistics.

5.3.1 Horizontal correlations

Table 2 shows that the average standard deviation for this case is very similar to that of Case 1. However, the correlation length scale is slightly reduced compared to Case 1 (Figure 3). This suggests that the use of superobservations may introduce some observation error correlation, but does not appear to be the main source of correlations.

Figure 4 shows that the standard deviations for individual elevations are similar to those found in Case 1. In general we find that the use of the thinned data results in slightly shorter observation error correlation length scales for observations that are at lower elevations and far range. For example, Figure 12 shows, for the 2^o elevation, that the use of the

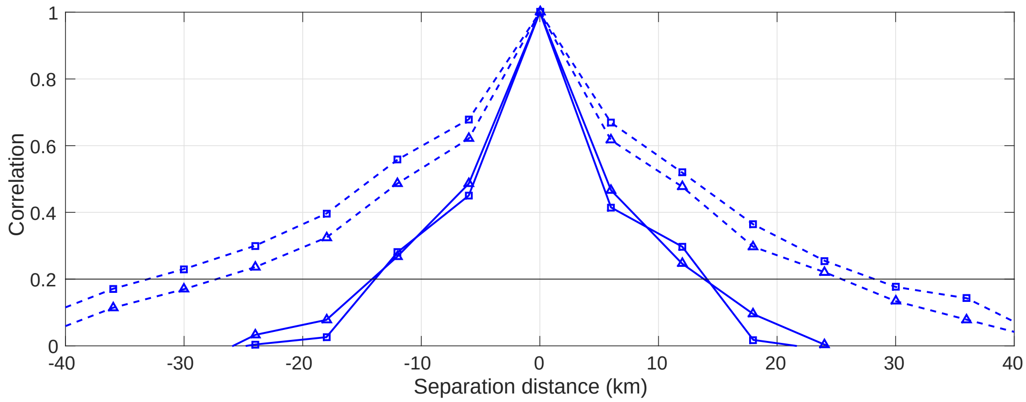

Figure 12 – Horizontal observation correlations for elevation 2^o at a range of 24km (solid) and 90km (dash) for Case 1 (control, squares) and Case 3 (Thinned raw data, triangles). Error correlations are deemed to be insignificant below the horizontal line at 0.2.

superobservtions has little impact on the correlation length scale at short range. However, at far range the correlation length scale for Case 1 is approximately 5km longer than that for Case 3. This result supports our hypothesis that the use of superobservations increases the observation error correlation length scale at far range. This is a result of the invalid assumption that the errors in the background states used in the superobservation creation are of the same magnitude and fully correlated.

5.3.2 Along-beam correlations

From Table 2 we see that the average along-beam observation error standard deviation is similar to that found using the data from Case 1. Figure 7 shows that the correlation length scale is also slightly reduced.

Figure 8 shows that the standard deviations for separate elevations are similar to Case 1. Figures 10 and 11 show that using the raw observations results in a similar shaped correlation function to Case 1 but with a slightly reduced length scale. The exception is the highest elevation (closest range) where the length scales are slightly larger. These results suggest that using the superobservation has the opposite effect, namely the introduction of correlation at far range, but a reduction of correlation in the higher elevations.

5.3.3 Summary

We have calculated observation error statistics using thinned raw observations. We find that:

- Using thinned raw data has little impact on the estimated observation error standard deviations; these are similar to Case 1.
- In general, horizontal correlation length scales at far range are slightly reduced. This implies that using superobservations introduces correlated error at far range, possibly as a result of an invalid assumption in the superobservation creation.
- In general along-beam correlation length scales are reduced for the lower elevations, however they slightly increased for the 6^o beam.

5.4 Case 4 - The effect of an improved observation operator

The previous cases have all used the simplified observation operator described in equation (6). The omission of the more complex terms introduces both additional error variance and correlation [Fabry, 2010]. It may not be possible to use a full observation operator in operational assimilation, though the use of the sophisticated observation operator in equation (11) may be considered. In this case we use this new observation operator to see if including beam broadening and reflectivity weighting in the observation operator has any affect on the observation error statistics. Here we use the thinned raw observations rather than the superobservations (the creation of the superobservation involves the observation operator, and ideally we wish to isolate the impact of the observation operator in the assimilation), hence the results here must be compared to Case 3.

5.4.1 Horizontal correlations

For the average horizontal error statistics both the standard deviation and correlation length scale have decreased compared to Case 3 (see Table 2 and Figure 3).

For the separate elevations, as with all previous cases, we find that the standard deviations increase with height (Figure 4), though here the actual values for the lower elevations are reduced compared to the standard deviations found in Case 3. The reduction is not seen in the higher elevations as observations are at near range where the effects of beam bending and broadening, accounted for in the new observation operator, are not so significant. In general we find that the correlations for every elevation are slightly decreased when using the improved observation operator (not shown). When considering horizontal correlations we compare observations at the same range away from the radar that have the same measurement volume, and hence the new observation operator should have the same improvement for each observation we compare. The reduction in error standard deviation and correlation shows that the inclusion of the beam broadening and reflectivity weighting has improved the observation operator. It also suggests that the use of an even more sophisticated observation operator may further reduce the observation error correlation.

5.4.2 Along-beam correlations

In this case Table 2 and Figure 8 show that the error standard deviation is reduced compared to Case 3 suggesting that the more sophisticated observation operator is indeed an improved map from background to observation space. Both Figure 7 and the correlations for separate elevations suggest that introducing the new observation operator slightly increases the correlation length scale. We hypothesize that this is a result of the inclusion of the beam broadening. When using the old observation operator observations at different ranges at any elevation were unlikely to consider data from the same model levels. With the introduction of the beam broadening different observations will now use information from the same model levels and this is likely to be the cause of the increased correlation length scales.

5.4.3 Summary

For this case we have calculated observation error statistics using thinned raw observations and an improved observation operator. We find that:

- Using the new observation operator reduces the error standard deviations for the lower elevations. Less impact is seen in the higher elevations where the effects of beam bending and broadening (accounted for in the new observation operator) are not so significant.
- For the horizontal correlations using the new observation operator reduces the estimated observation correlation length scale. This suggests that error in the observation operator may be in part responsible for the large correlation length scales.
- Using the new observation operator increases the along-beam correlation. This is likely to be the result of close observation residuals sharing increased amounts of background data.

6 Conclusions

With the development of convection-permitting NWP the assimilation of high resolution observations is becoming increasingly important. To use the observations to their full potential their associated error statistics must be well understood and correctly specified. Observation errors can be attributed to a number of different sources, some of which may be state dependent and dependent on the model resolution. Calculation of observation error statistics is difficult as they cannot be measured directly. Recently the diagnostic of Desroziers et al. [2005] has been used to estimate inter-channel observation error correlations for a number of different observation types. In this work we use the diagnostic to estimate spatially correlated errors for Doppler radar radial wind (DRW) observations that are assimilated into the Met Office UKV model. Errors for DRWs may be correlated horizontally, vertically or along the path of the radar beam. In this work we consider both the horizontal and along-beam error statistics.

Initially error statistics were calculated for observations assimilated into the UKV model operational in January 2014. This provided information on the general structure of the observation errors and how they vary throughout the atmosphere. Error statistics were also calculated using data from an assimilation run using alternative background error statistics. This provided information on how sensitivity of the results to the specification of the background error statistics. The diagnostic was then applied to data from a further two assimilation runs. These evaluated the impact that the use of superobservations and errors in the observation operator have on the estimated observation error statistics.

Results from all four cases showed similar behaviour for the estimated statistics. We are able to conclude that most DRW error standard deviations, horizontal and along-beam correlation length scales increase with height, as a function of the increase in measurement volume. Thus at least part of the correlated errors are likely to be related to the uncertainty in the observation operator. The exceptions are the standard deviations at the lowest heights. Observations at the lowest heights have the smallest measurement volumes, smaller than the model grid spacing, and hence representativity errors may well account for the larger standard deviations at lower heights.

Results showed that the estimated standard deviations are similar those used operationally. However for the majority of cases, with exception of the 6^o beam, the correlation length scales are much larger than those found in Simonin et al. [2012] and the operational thinning distance of 6km. Despite the differences in operational system, our estimated average along-beam correlations are similar to those calculated by Météo-France [Wattrelot et al., 2012]. Furthermore, observation error statistics estimated when using an alternative background error covariance matrix in the assimilation and the results from Waller et al. [2015] imply that the observation error correlation length scale is underestimated. This suggests that the errors are correlated to a degree that it should be accounted for in the assimilation.

In an attempt to understand the source of the error correlations, the effect of using superobservations and an improved observation operator are considered. The use of the superobservations does not affect the error standard deviations. However, results suggest that the use of superobservations introduces correlated error at far range, possibly as a result of an invalid assumption in the superobservation creation. The use of an improved observation operator reduces the error standard deviations, particularly at low elevations and at far range where observations have large measurement volumes. This is expected since the new observation operator takes into account the beam broadening and bending, both of which affect the beam most at far range. The improvement in the low elevations is related to the inclusion in the observation operator of information from more model levels. These are denser in the lower atmosphere where the low elevations provide observations. The use of the new observation operator results in an increase of the along-beam correlation length scale. We hypothesize that this is a result of nearby observation residuals now sharing information from the same model levels. However, the horizontal correlations were slightly reduced. This suggests not only that some of the horizontal correlations previously seen were a result of omissions in the observation operator, but also that the horizontal correlation length scale may be further reduced with the use of on even more complex observation operator.

These results provide a better understanding of DRW observation error statistics and the sources that contribute to them. We have shown that these observation errors exhibit large spatial correlations that are much larger that the operational thinning distance. This implies that either the data must be thinned further to ensure the errors are uncorrelated or the correlated errors must be accounted for in the assimilation.

Acknowledgments

This work is funded in part by the NERC Flooding from Intense Rainfall programme and the NERC National Centre for Earth Observation.

References

S. Ballard, Z. Li, D. Simonin, and J.-F. Caron. Performance of 4D-Var NWP-based nowcasting of precipitation at the Met Office for summer 2012. *Submitted to Quarterly Journal of the Royal Meteorological Society*, 2015.

H. Berger and M. Forsythe. Satellite wind superobbing. Technical report, Met Office, UK, 2004. Forecasting Research Technical Report 451.

V. Bondarenko, T. Ochotta, and D. Saupe. The interaction between model resolution, observation resolution and observations density in data assimilation: A two-dimensional study. *Preprints, 11th Symp. on Integrated Observing and Assimilation Systems for the Atmosphere, Oceans, and Land Surface, San Antonio, TX, Amer. Meteor. Soc., P5.19.*, 2007. Available online at http://ams.confex.com/ams/pdfpapers/117655.pdf.

N. Bormann and P. Bauer. Estimates of spatial and interchannel observation-error characteristics for current sounder radiances for numerical weather prediction. I: Methods and application to ATOVS data. *Quarterly Journal of the Royal Meteorological Society*, 136: 1036–1050, 2010.

N. Bormann, A. Collard, and P. Bauer. Estimates of spatial and interchannel observation-error characteristics for current sounder radiances for numerical weather prediction. II: Application to AIRS and IASI data. *Quarterly Journal of the Royal Meteorological Society*, 136:1051–1063, 2010.

P. Courtier, J. Thepaut, and A. Hollingsworth. A strategy for operational implementation of 4D-var,using an incremental approach. *Quarterly Journal of the Royal Meteorological Society*, 120:1367–1387, 1994.

S. L. Dance. Issues in high resolution limited area data assimilation for quantitative precipitation forecasting. *Physica D: Nonlinear Phenomena*, 196:1 – 27, 2004.

D. P. Dee and A. M. Da Silva. Maximum-likelihood estimation of forecast and observation error covariance parameters. Part I: Methodology. *Monthly Weather Review*, 127:1822–1843, 1999.

G. Desroziers, L. Berre, B. Chapnik, and P. Poli. Diagnosis of observation, background and analysis-error statistics in observation space. *Quarterly Journal of the Royal Meteorological Society*, 131:3385–3396, 2005.

R. J. Doviak and D. S. Zrnic. *Doppler Radar and Weather Observations*. Academic Press, second edition, 1993.

F. Fabry. Radial velocity measurement simmulations: common errors, approimations, or ommissions and their impact on estimation accuracy. *In Proceedings of of the sixth European conference on radar in meteorology and hydrology*, 2010.

S. B. Healy and A. A. White. Use of discrete Fourier transforms in the 1D-Var retrieval problem. *Quarterly Journal of the Royal Meteorological Society*, 131:63–72, 2005.

A. Hollingsworth and P. Lönnberg. The statistical structure of short-range forecast errors as determined from radiosonde data. Part I: The wind field. *Tellus*, 38A:111–136, 1986.

T. Janjic and S. E. Cohn. Treatment of observation error due to unresolved scales in atmospheric data assimilation. *Monthly Weather Review*, 134:2900–2915, 2006.

M. Kitchen. Towards improved radar estimates of surface precipitation rate at long range. *Quarterly Journal of the Royal Meteorological Society*, 123:145163, 1997.

H. Lean, P. Clark, M. Dixon, N. Roberts, A. Fitch, R. Forbes, and C. Halliwell. Charictaristics of high-resolution versions of the Met Office Unified Model for forecasting convection over the United Kingdom. *Monthly Waether Review*, 136:3408–3424, 2008.

Z. Li, S. Ballard, and D. Simonin. Comparison of 3D-Var and 4D-Var data assimilation in an NWP-based nowcasting system of precipitation at the Met Office. *Quarterly Journal of the Royal Meteorological Society*, 2015.

M. Lindskog, H. Jarvinen, and D. B. Michelson. Assimilation of radar radial winds in the HIRLAM 3D-Var. *Physics and Chemistry of the Earth - Part B: Hydrology, Oceans and Atmosphere*, 25:1243–1249, 2000.

M. Lindskog, N. Gustafsson, B. Navascues, K. S. Mogensen, X. Y. Huang, X. Yang, U. Andrae, L. Berre, S. Thorsteinsson, and J. Rantakokko. Three-dimensional variational data assimilation for a limited area model. Part II: Observation handling and assimilation experiments. *Tellus*, 53A:447–468, 2001.

M. Lindskog, K. Salonen, H. Jaarvinen, and D. B. Michelson. Doppler radar wind assimilation with HIRLAM 3DVAR. *Monthly Weather Review*, 132:1081–1092, 2004.

Z.-Q. Liu and F. Rabier. The interaction between model resolution observation resolution and observation density in data assimilation: A one dimensional study. *Quarterly Journal of the Royal Meteorological Society*, 128:1367–1386, 2002.

A. C. Lorenc, S. P. Ballard, R. S. Bell, N. B. Ingleby, P. L. F. Andrews, D. M. Barker, J. R. Bray, A. M. Clayton, T. Dalby, D. Li, T. J. Payne, and F. W. Saunders. The met. office global three-dimensional variational data assimilation scheme. *Quarterly Journal of the Royal Meteorological Society*, 126:2991–3012, 2000.

T. Montmerle and C. Faccani. Mesoscale assimilation of radial velocities from Doppler radars in a preoperational framework. *Monthly Weather Review*, 137:1939–1953, 2009.

S. K. Park and D. Zupanski. Four-dimensional variational data assimilation for mesoscale and storm-scale applications. *Meteorology and Atmospheric Physics*, 82:173–208, 2003.

C. Piccolo and M. Cullen. Adaptive mesh method in the Met Office variational data assimilation system. *Quarterly Journal of the Royal Meteorological Society*, 137:631–640, 2011. doi: 10.1002/qj.801.

C. Piccolo and M. Cullen. A new implementation of the adaptive mesh transform in the Met Office 3D-Var system. *Quarterly Journal of the Royal Meteorological Society*, 138: 1560–1570, 2012. doi: 10.1002/qj.1880.

F. Rawlins, S. P. Ballard, K. J. Bovis, A. M. Clayton, D. Li, G. W. Inverarity, A. C. Lorenc, and T. J. Payne. The Met Office global four-dimensional variational data assimilation scheme. *Quarterly Journal of the Royal Meteorological Society*, 133:347–362, 2007.

S. J. Rennie, A. J. Illingworth, S. L. Dance, and S. P. Ballard. The accuracy of doppler radar wind retrievals using insects as targets. *Meteorological Applications*, 17:419 – 432, 2010. doi: 10.1002/met.174.

S. J. Rennie, S. L. Dance, A. J. Illingworth, S. P. Ballard, and D. Simonin. 3D-Var assimilation of insect-derived Doppler radar radial winds in convective cases using a high-resolution model. *Monthly Weather Review*, 139:1148–1163, 2011.

F. A. Rihan, C. G. Collier, S. P. Ballard, and S. J. Swarbrick. Assimilation of Doppler radial winds into a 3d-var system: Errors and impact of radial velocities on the variational analysis and model forecasts. *Quarterly Journal of the Royal Meteorological Society*, 134: 1701–1716, 2008.

K. Salonen, H. Jarvinen, R. Eresmaa, and S. Niemela. Bias estimation of Doppler radar radial-wind observations. *Quarterly Journal of the Royal Meterological Society*, 133: 1501–1507, 2007.

K. Salonen, H. Jarvinen, S. Jarvenoja, S. Niemela, and R. Eresmaa. Doppler radar radial wind data in nwp model validation. *Meteorological Applications*, 15:97–102, 2008.

K. Salonen, H. Jarvinen, G. Haase, S. Niemela, and R. Eresmaa. Doppler radar radial winds in HIRLAM. Part II: Optimizing the super-observation processing. *Tellus*, 61A: 288–295, 2009.

D. Simonin. New implementation for the assimilation of Doppler radial wind observations. Technical report, Met Office, UK, 2014. Progress Report.

D. Simonin, S. Ballard, Z. Li, and J. F. Caron. Doppler radar assimilation. ERAD 201 27th European Conference on Radar in Meteorology and Hydrology, June 2012. http://www.meteo.fr/cic/meetings/2012/ERAD/presentations/friday/14-2.pdf.

D. Simonin, S. P. Ballard, and Z. Li. Doppler radar radial wind assimilation using an hourly cycling 3D-Var with a 1.5 km resolution version of the Met Office Unified Model for nowcastings. *Quarterly Journal of the Royal Meteorological Society*, 2014. doi: 10.1002/qj.2298.

L. M. Stewart. *Correlated observation errors in data assimilation*. PhD thesis, University of Reading, 2010. http://www.reading.ac.uk/maths-and-stats/research/theses/maths-phdtheses.aspx.

L. M. Stewart, S. L. Dance, and N. K. Nichols. Correlated observation errors in data assimilation. *International Journal for Numerical Methods in Fluids*, 56:1521–1527, 2008.

L. M. Stewart, J. Cameron, S. L. Dance, S. English, J. R. Eyre, and N. K. Nichols. Observation error correlations in IASI radiance data. Technical report, University of Reading, 2009. Mathematics reports series, www.reading.ac.uk/web/FILES/maths/obs_error_IASI_radiance.pdf.

L. M. Stewart, S. L. Dance, and N. K. Nichols. Data assimilation with correlated observation errors: experiments with a 1-D shallow water model. *Tellus A*, 65, 2013. doi: http://dx.doi.org/10.3402/tellusa.v65i0.19546.

L. M. Stewart, S. L. Dance, N. K. Nichols, J. R. Eyre, and J. Cameron. Estimating interchannel observation-error correlations for IASI radiance data in the Met Office system. *Quarterly Journal of the Royal Meteorological Society*, 140:1236–1244, 2014. doi: 10.1002/qj.2211.

J. Sun. Convective-scale assimilation of radar data: Progresses and challenges. *Quarterly Journal of the Royal Meteorological Society*, 131:3439–3463, 2005.

J. Sun, M. . Xue, J. W. Wilson, I. Zawadzki, S. P. Ballard, J. Onvlee-Hooimeyer, P. Joe, D. M. Barker, P.-W. Li, B. Golding, M. Xu, and J. Pinto. Use of NWP for nowcasting convective precipitation: Recent progresses and challenges. *Bulletin of the American Meteorological Society*, 95:409–426, 2014.

Y. Tang, H. W. Lean, and J. Bornemann. The benefits of the Met Office variable resolution NWP model for forecasting convection. *Meteorological Applications*, 20:417–426, 2013. doi: 10.1002/met.1300.

J. Toomay and P. Hannen. *Radar Principles for the Non Specialist*. SciTech Publishing, third edition, 2004.

J. A. Waller. *Using observations at different spatial scales in data assimilation for environmental prediction*. PhD thesis, University of Reading, Department of Mathematics and Statistics, 2013. http://www.reading.ac.uk/maths-and-stats/research/theses/maths-phdtheses.aspx.

J. A. Waller, S. L. Dance, A. S. Lawless, and N. K. Nichols. Estimating correlated observation error statistics using an ensemble transform Kalman filter. *Tellus A*, 2014a. doi: http://dx.doi.org/10.3402/tellusa.v66.23294.

J. A. Waller, S. L. Dance, A. S. Lawless, N. K. Nichols, and J. R. Eyre. Representativity error for temperature and humidity using the Met Office high-resolution model. *Quarterly Journal of the Royal Meteorological Society*, 140:1189–1197, 2014b. doi: 10.1002/qj.2207.

J. A. Waller, S. L. Dance, and N. K. Nichols. Theoretical insight into diagnosing observation error correlations using observation-minus-background and observation-minus-analysis statistics. *Quarterly Journal of the Royal Meteorological Society*, 2015. accepted.

E. Wattrelot, T. Montmerle, and C. G. Guerrero. Evolution of the assimilation of radar data in the arome model at convective scale. *In Proceedings of of the seventh European conference on radar in meteorology and hydrology*, 2012.

P. P. Weston, W. Bell, and J. R. Eyre. Accounting for correlated error in the assimilation of high-resolution sounder data. *Quarterly Journal of the Royal Meteorological Society*, 2014. doi: 10.1002/qj.2306.

Q. Xiao, Y. H. Kuo, J. Sun, W. C. Lee, E. Lim, Y. R. Guo, and D. M. Barker. Assimilation of Doppler radar observations with a regional 3D-VAR system: Impact of Doppler velocities on forecasts of a heavy rainfall case. *Journal of Applied Meteorology*, 44:768–788, 2005.

Q. Xiao, J. Sun, W. C. Lee, Y. H. Kuo, D. M. Barker, E. Lim, D. J. Won, M. S. Lee, W. J. Lee, J. Y. Cho, D. K. Lee, and H. S. Lee. Doppler radar data assimilation in KMAs operational forecasting. *Bulletin of the American Meteorological Society*, 89:39–43, 2008.

Q. Xu, K. Naib, and L. Weib. An innovation method for estimating radar radial-velocity observation error and background wind error covariances. *Quarterly Journal of the Royal Meteorological Society*, 133:407–415, 2007.